Design and Development of a Torsional Thrust Stand for mNs Thrust Measurements

IEPC-2022-170

Presented at the 37th International Electric Propulsion Conference
Massachusetts Institute of Technology, Cambridge, MA USA
June 19-23, 2022

Mohammed Asif[1], Hannah L. Watts [2], Nathaniel J. Allwine[3], Luke Fouch[4], Jeremy Baiocchi[5], Logan Hefferan[6], Douglas Adams[7], and Kristina Lemmer[8]

Western Michigan University, College of Engineering and Applied Science, Kalamazoo, MI, 49009 United States

This paper presents progress towards the development of a torsional thrust stand that was designed at Western Michigan University's Aerospace Laboratory for Plasma Experiments (ALPE). The paper highlights design decisions for the individual subsystems associated with the thrust stand to achieve direct thrust measurements in the range of 1 to 100 mN with a resolution of 0.1 mN and a mean noise magnitude of 0.8 µm. The current version of the thrust stand design includes a manual leveling system, a passive Eddy current damping system, and a fiber optic laser displacement sensor. Calibration testing was performed in a vacuum chamber with a base pressure of approximately 10^6 Torr to create a calibration curve in the 20 to 80 mN range with a sensitivity of 1µm/mN.

I. Nomenclature

c = Damping coefficient
k = Spring coefficient
I = Moment of intertia
$\theta(t)$ = Arm rotation
$\dot{\theta}$ = Angular velocity
$\ddot{\theta}$ = Angular acceleration
ζ = Damping ratio
ω_n = Natural frequency
L_t = Length of thrust arm
F_t = Thrust force
$\mathrm{F}_{\mathrm{eddy}}$ = Eddy current force
S = Surface area of conductive material
B = Magnetic field strength
V = Relative arm velocity to magnet
σ = Conductive coefficient
δ = Conductive material thickness

[1] Ph.D. Student, Mechanical and Aerospace Engineering, mohammed.asif@wmich.edu
[2] Graduate Student, Mechanical and Aerospace Engineering, hannah.l.watts@wmich.edu
[3] Graduate Student, Mechanical and Aerospace Engineering, nathaniel.j.allwine@wmich.edu
[4] Undergraduate Student, Mechanical and Aerospace Engineering, luke.w.fouch@wmich.edu
[5] Undergraduate Student, Mechanical and Aerospace Engineering, jeremy.baiocchi@wmich.edu
[6] Undergraduate Student, Mechanical and Aerospace Engineering, logan.s.hefferan@wmich.edu
[7] Undergraduate Student, Mechanical and Aerospace Engineering, douglas.j.adams@wmich.edu
[8] Associate Professor, Mechanical and Aerospace Engineering, kristina.lemmer@wmich.edu

Δx_{ss} = Measured displacement from a steady-state thruster
S_{cal} = Sensitivity
F_{cal} = Known force from calibration weights
L_{pm} = Length between thruster and pendulum pivot
L_{cal} = Length between calibration weights and pendulum pivot

II. Introduction

Electric propulsion (EP) has seen a steady increase in popularity as a result of both technological advancements and the progress of more affordable satellite missions. One of the key factors for determining performance capability for new EP devices is the force of thrust provided to a spacecraft. The methods traditionally used for gauging this metric of performance for chemical rockets differ significantly from those required to measure thrust in most EP devices due to the low thrust-to-mass ratios of most EP devices. Thrust can be calculated using data collected via plasma diagnostic tools such as the Langmuir probes, Faraday cups, and retarding potential analyzers [1–4]. However, these diagnostic tools must be in physical contact with the plasma plume and can influence plume characteristics, causing inconsistencies since slight variations in the plasma plume can have an impact on performance metrics such as efficiency and mass utilization. Additionally, EP devices with a passive propellant mass flow do not currently have an accurate and time-resolved method for measuring mass flow rate of propellant out of the thruster, preventing the true estimation of thrust performance metrics from plume measurements. Furthermore, there are inefficiencies that cannot be measured with plasma diagnostics and operational telemetry. Therefore, the best method for measuring thruster performance is to get a direct thrust measurement from a thrust stand. The development of an affordable, modular thrust stand capable of directly measuring the force produced by a thruster while preserving the integrity of the plasma plume is necessary for the burgeoning EP developments at Western Michigan University (WMU) and other academic institutions.

This work presents progress on the design, development, and calibration testing of a modular, mN torsional thrust stand developed at the Aerospace Laboratory for Plasma Experiments (ALPE) at WMU. The thrust stand presented here is necessary for future EP work at ALPE and will provide a blueprint for other academic institutions. Section III provides general background on thrust stand design, section IV highlights the thrust stand design decisions, section V presents results from experimental testing and calibration, and section VI concludes the paper with future work.

III. Background

The pendulum thrust stand is a variation of the simple spring-mass-damper system to ensure accurate steady-state and impulse thrust measurements. Therefore, any pendulum thrust stand can be modeled by the equation of motion:

$$I\ddot{\theta} + c\dot{\theta} + k\theta(t) = F_t L_t \tag{1}$$

which is expressed in standard terms as

$$\ddot{\theta} + 2\zeta\omega_n\dot{\theta} + \omega_n^2\theta(t) = F_t L_t / I \tag{2}$$

The three major configurations for pendulum-type thrust stands are hanging pendulum, inverted pendulum, and torsional pendulum. While all three types utilize some sort of spring-mass-damper system, they each have unique advantages and disadvantages when pairing the right thrust stand for the thruster. Fig. 1 below shows the different pendulum configurations [6].

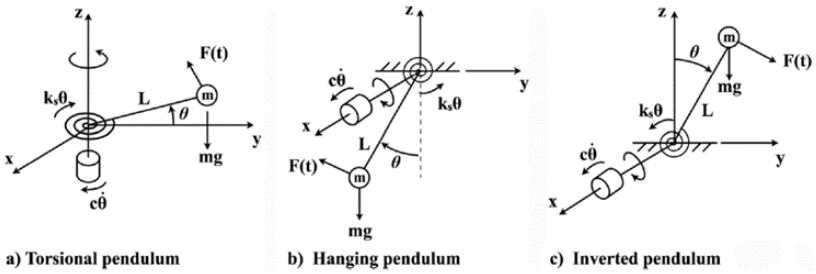

Fig. 1 Different pendulum configurations used in a pendulum the thrust stand [5]

The primary difference between these types of thrust stands is the way that gravitational forces interact with the entire system dynamics. In the case of the hanging pendulum, the gravitational force acts more as the restoring force; whereas, in the inverted pendulum stand, the gravitational force increases the deflection. For the torsional pendulum, gravity does not play a role in the deflection given that the direction of deflection is perpendicular to the plane of motion. The dynamic system model, solved from Eqn. (2), is illustrated in Eqn. (3) for underdamped, critically damped, and overdamped situations.

$$\frac{\theta(t) I \omega_n^2}{F_t L_t} = \begin{cases} 1 - e^{-\zeta \omega_n t}\left[\cos(\omega_d t) + \dfrac{\zeta}{\sqrt{1-\zeta^2}}\sin(\omega_d t)\right] & if\ \zeta < 1 \\ 1 - e^{-\omega_n t}(1 - \omega_n t) & if\ \zeta = 1 \\ 1 + \dfrac{1}{2\sqrt{\zeta^2 - 1}}\left[\dfrac{1}{d_1} e^{-d_1 \omega_n t} - \dfrac{1}{d_2} e^{-d_2 \omega_n t}\right] & if\ \zeta > 1 \end{cases} \tag{3}$$

Six primary identified performance metrics influence the quality of a thrust measurement. Optimizing and characterizing these parameters will directly influence thrust stand performance [5].

• Sensitivity: Sensitivity can be seen as the deflection that is shown as a force is applied by a steady state thruster system. This is one of the most important features as the base thrust generated by electric propulsion devices is usually in the micronewton range. This also directly influences the precision and resolution of the measurement.

• Repeatability and Long-Term Stability: The measured thrust from the sensitivity must be repeatable over time such that the value is stable enough to record the thrust produced and not the noise. Repeatability reflects and directly influences accuracy. The long-term stability can be affected by the pendulum system. Therefore, a calibration system is required to account for the pre-post measurement operation.

• Accuracy: The error margin between measured thrust and actual thrust offers the accuracy of the thrust stand. This is different from the sensitivity, which covers the precision of the system.

• Resolution: The resolution refers to the lowest thrust value that can be recognized by the thrust stand system. Lower resolution is better for steady low thrust engines.

• Response Time: The response time is given as a way to characterize time-resolved measurements. Harmonics, thruster noise, time required to reach a peak response, and changes in the steady state operation will result in a different response time.

• Predictability of the Response: The ideal response is said to be linear, but this is not a necessity as small angle deflections can be changed based on the spring, damper, and sensors. Although Polk et. al [5-6], recommend a linear design over a non-linear one.

IV. Thrust Stand Design

For the rest of this paper, the term 'thrust stand' refers to the torsional pendulum stand developed at ALPE. As this is the first thrust stand developed in-house at ALPE, modularity of the design to test the multiple types of EP and pulsed cold gas thrusters is important. However, the initial goal of the project is to adapt the thrust stand to accommodate a cold gas thruster for a CubeSat mission with a pulsed thrust output in the mN range. Accuracy, compatibility, size, cost, and tailoring for the vacuum environment drove the design criteria for each design parameter. Also, the thrust stand is intended to be as economical as possible with design considerations such that it can be replicated relatively inexpensively. Furthermore, dimensional limitations based on the size of the vacuum facility at ALPE (1.5-m-long by 1-m-diameter) must be accommodated. An aluminum mounting frame is seated within the cylindrical chamber to ease in the setup of the vast number of experiments for which the chamber is used; therefore, the useable space for the thrust stand is 78.74 x 15.748 x 9.65 centimeters (L x W x H). The vacuum chamber is capable of reaching base pressures of 1e-7 Torr.

Primary design considerations were organized into five discrete categories for ease of understanding. Fig. 2 shows the design of the thrust stand that was modeled after the torsional thrust stand built by Haag [7].

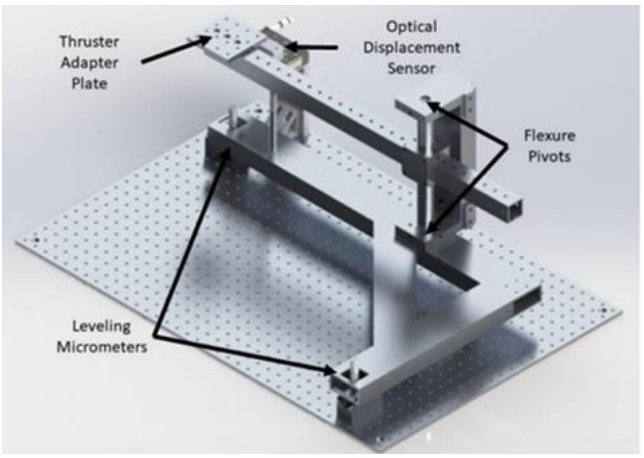

Fig. 2 Initial 3D rendering of the thrust stand design

A. Base Structure, Leveling System, and Torsional Arm

The main considerations observed in the design of the thrust stand structure were ease of manufacturing, stability control, and dimensional constraints. An L-shaped base support was chosen where the right-angle corner is fixed to the base plate, necessitating a two-point leveling system to account for variance in both the x and y dimensions. A cross beam is used to limit system perturbations induced by general vibrations in the testing environment. Leveling is achieved with manually adjusted micrometers, as shown in Fig 3.

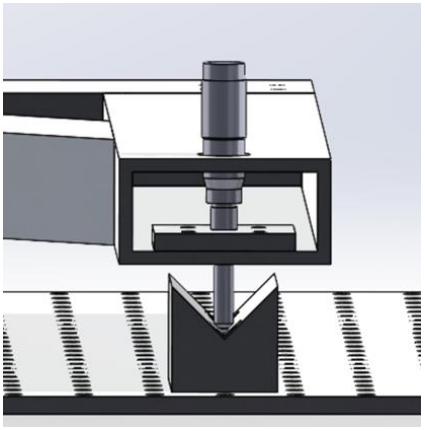

Fig. 3 CAD of the leveling system

A decision matrix, Table 1 was used to select the micrometer from a variety of commercially available products. For this and other decision matrices in this paper, a 1-4 scale was used to indicate the fitness of the design for the selection criteria, with a high score representing a good fit and a low score showing a poor fit. Using the following decision matrix, the SM-25 Micrometer was selected and installed due to its balance of affordability, travel distance, load capacity, and size. Since a manual leveling system was selected, in-situ adjustments are not possible. Therefore, an Analog Devices ADIS16209 inclinometer was implemented to monitor the stability of the thrust stand during vacuum experiments. This leveling verification process has yet to be tested in vacuum.

Table 1 Leveling decision matrix

	PIAK10VF	Z806-V	8301-V	N-111.201	SM-13	SM-25	MH-2500
Cost	1	1	1	1	4	4	3
Travel Distance	3	4	3	3	3	4	3
Max Load Capacity	2	2	3	4	2	4	2
Size	4	4	4	3	4	4	2
Total	10	11	11	11	13	16	10

The main torsional system employs a two-piece system that fits together as shown in Fig. 4. The torsional arm is designed to be modular such that the ratio of thruster arm length to counter arm length can be adjusted based on dynamic model optimization calculations for each thruster tested.

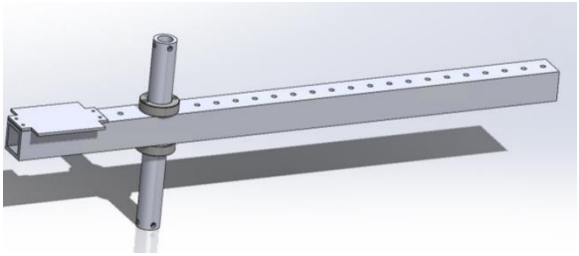

Fig. 4 Design of the main torsional arm and flexure rod

B. Damping System

Magnetic damping systems are the modern standard in common thrust stand systems due to vacuum environment restrictions, primarily outgassing [8]. The primary design consideration for the damping system is the damping coefficient, ζ, which was tuned to an underdamped mode such that $0.4 < \zeta < 0.8$ to achieve an optimal steady-state response for taking experimental measurements [5]. To tune the damping coefficient and ensure adding as little complexity as possible to the dynamic model, a magnetic damping system was chosen that utilized the force produced by Eddy currents formed on a copper plate by a magnetic source to achieve the desired damping effects.

The resistive force that an Eddy current imparts on a system is a function of the conductive properties of a copper plate, the velocity of the magnet in relation to that plate, and the magnetic field strength. This is found using Eqn. (4).

$$\mathrm{F_{eddy}} = -\sigma\delta \mathrm{S V B^2} \tag{4}$$

Combining Eqn. (4) with the second-order, underdamped model given in Eqn. (3), yields an estimate of the magnetic field required to produce the necessary damping coefficients as

$$B = \sqrt{\frac{2I\zeta\sqrt{\frac{2k}{I}}}{\sigma\delta S}} \tag{5}$$

Initially, an electromagnet was considered to generate the necessary Eddy currents in the copper plate. Through control of the current running through the electromagnet, the damping constant could be precisely tuned for different thrust levels. Unfortunately, a poorly designed electromagnet resulted in overheating, and a permanent magnet design was implemented. The damping system uses an N52 Neodymium magnet suspended in a central position over a copper plate. The distance between the magnet and copper plate is adjustable by a linear motion table such that the B-field applied to the plate can be adjusted. Therefore, the damping constant can be varied in the dynamic system model. The distribution of the magnetic field is shown in Fig. 5. The experimental measurements were taken with a gauss meter that would periodically be moved away from the magnet. The theoretical data were taken from the distributer K & J magnetics. The corresponding magnetic field strength for a range of desirable damping constants is shown in Table 2 below. This was crucial in selecting the right grade and size of neodymium magnet.

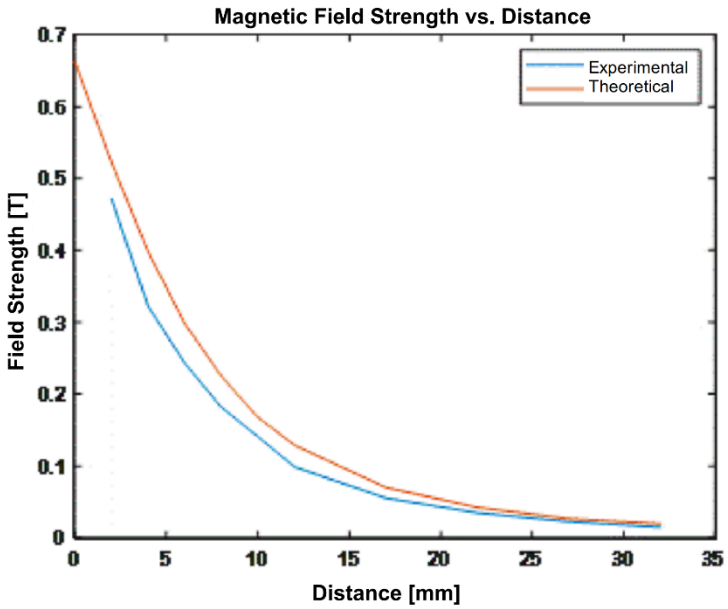

Fig. 5 B-Field Distribution of 19.05mm x 19.05mm disc magnet

Table 2 Magnetic field strength for corresponding damping constants

Damping	Magnetic Field Strength [T]	Damping Constant
0.4	0.27	0.81
0.5	0.03	1.01
0.6	0.36	1.21
0.7	0.36	1.42
0.8	0.38	1.62

C. Flexure System

In torsional thrust stand design and manufacturing, flexure pivots are used to allow for rotation of the torsion arm about an axis with a known spring constants. The designed presented utilizes two flexure pivots arranged co-axially on the flexure rod, one above, and one below the torsion arm, as seen in Fig. 4.

The required flexure pivot specifications were acquired from the maximum measured thrust requirement of 100 mN and the desired resolution of 1 mN. The decision matrix shown in Table 3 shows that the I-30 flexure pivot from C-flex is the best option for this design. The I-30 Flexure Pivot has a known torsional spring rate of 3.261 in*lb/deg and a maximum torsional angle of +/- 7.5 degrees.

Table 3 Flexure pivot decision matrix

	G-30	H-30	I-30	J-30
Cost	4	3	3	2
Diameter Fit	2	3	4	1
Max. Deflection	2	3	3	1
Spring Constant	2	3	3	1
Max Radial Loading	1	2	3	4
Earliest Availability	1	4	4	1
Total	12	18	20	10

D. Displacement Sensor

The decision matrix for the selection of an optical sensor and corresponding vacuum feed-thru is provided in Table 4 below. The sensor selected for this design was Philtec Inc's mDMS-D64 shown in Fig. 6. This sensor can measure displacements ranging from 0.3 nm to 400 nm (peak-to-peak resolution), depending on sampling rate and the number of readings that are averaged. The mDMS-D64 is connected to Philtec's BV-133 Swagelok-fitted feedthrough to record measurements while in high vacuum. The optical sensor is mounted to the base of the thrust stand assembly independently from the stand's structure to reduce potential vibration and harmonic effects. The sensor probe is seated in an adjustable V-channel to allow for optimal performance at different steady-state displacements.

Table 4 Fiber optic displacement sensor matrix

	mDMS-47	mDMS-63	mDMS-64	mDMS-100
Cost	2	3	3	2
Vacuum Rating	4	4	4	4
Operating Range	3	2	4	4
Total	9	9	11	10

Fig. 6 Optical sensor mounted to thrust stand assembly

E. Calibration System

In-situ effects, including flowing current and thermal effects, contribute to the dynamic system model for thrust calculation. Rather than directly attempting to incorporate these unknown factors into the model, a known force calibration of the thrust stand can be performed. To correct for errors in the general dynamic system model and directly determine a thrust force from the measured displacement, a good calibration system must be implemented. Additionally, the thrust stand performance metrics of accuracy, precision, and repeatability are determined by this application of a known force.

A common calibration system applies forces by loading and unloading weights of known masses on a string that is rigged over a pulley that is attached to the torsional arm at a known distance from the pivot axis. A motor-driven spool is commonly used to adjust the applied force [5]. Fig. 7 shows the calibration system designed for the ALPE thrust stand, where weight loading is accomplished using a vertically positioned motion stage with a mounted weight "collector cup" to adjust the applied load on the torsional arm. This decision was made to reduce the potential effects the free-hanging weights and spool mechanism could have on the precise force applied to the arm. The weights attached to the fine string were separated by a common distance to make the force application process easier. The known force was placed at a distance of 20.32 cm from the rotational axis. As a result of space constraints, only four weight stages were developed. In ideal circumstances, additional weight stages would be implemented.

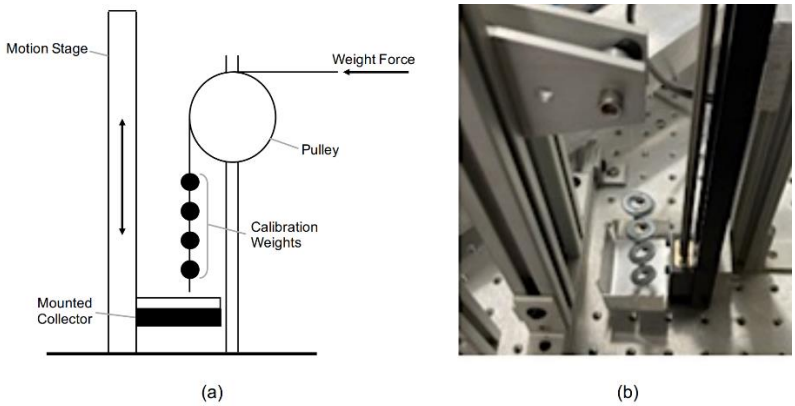

Fig. 7 (a) Schematic of the calibration system (b) Final calibration system design

Assuming the torsion arm is static under load, the moment produced by the known calibration force and the thrust force can be equated. This relation is used to estimate the thrust stand sensitivity from the calibration fit given by

$$S_{cal} = \frac{\Delta x_{ss}}{F_{cal}} = \frac{L_{pm} L_{cal}}{I \omega_n^2} \tag{6}$$

From this estimation of sensitivity, the steady-state thrust is calculated from an experimentally measured displacement. Any uncertainty in the measurements of calibration distance and thruster distance from the pivot must be included in estimations of total uncertainty. The thrust equation is given by

$$F_t = \frac{(F_{cal}/L_t)}{S_{cal}} \Delta x_{ss} \tag{7}$$

V. Results

Vacuum testing of the thrust stand calibration system was performed in the vacuum chamber at ALPE with a base pressure of approximately 10^{-6} Torr. Calibration experiments were performed at damping coefficient values of approximately $\zeta = 0.3$, $\zeta = 0.4$, and $\zeta = 0.5$. The lack of accuracy in targeting exact damping coefficients was a result of the relatively large step distance of the motion table that moves the permanent magnet in the damping system. The current motion table used for testing both magnet actuation and calibration staging have a screw precision of 0.1 mm and a range of 200 mm. Fig. 8 shows the thrust stand being setup in the vacuum chamber for testing.

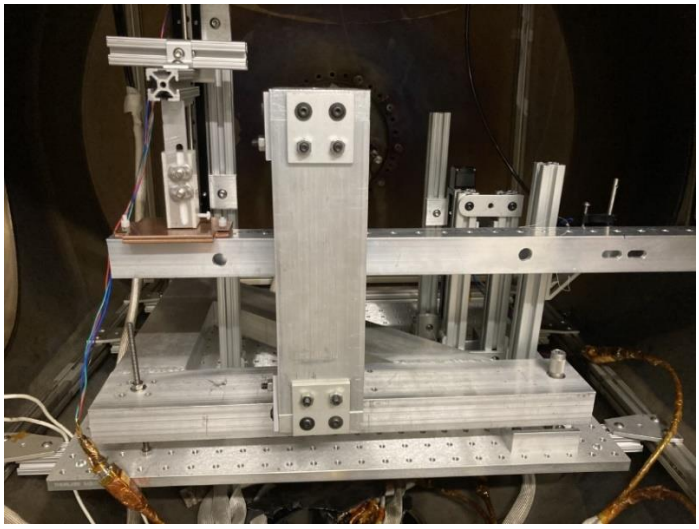

Fig. 8 Thrust stand inside of vacuum chamber for calibration experiments

To obtain the values used in following results, the displacement measured on each step plateau was averaged over at least 300 measurements to mitigate the effects of noise. A theoretical thruster positioned 30.48 cm off the rotational axis yields a theoretical sensitivity of 71 μN. In practice, outside disturbances and general noise will be the true limiting factor of a thrust stand's sensitivity. The calibration measurements also revealed that the minimum noise in displacement measurement was 0.8 μm due to vacuum chamber vibration. The step response data for the known calibration forces were consolidated and are shown in Fig. 9.

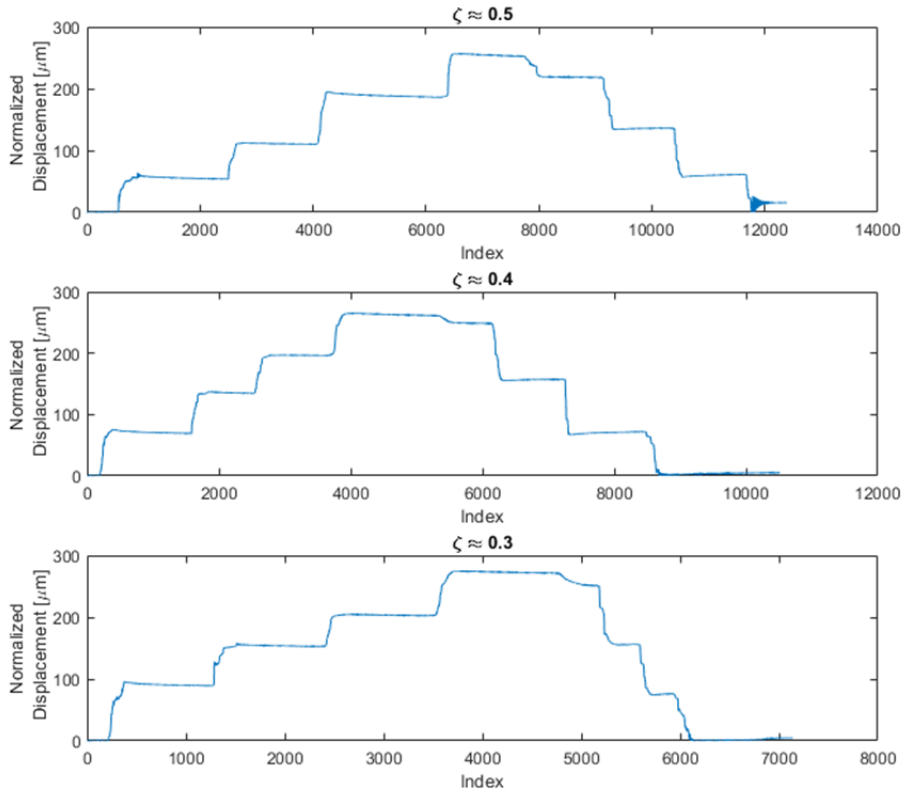

Fig. 9 Thrust stand calibration test step response to known application of force

Table 5 Numerical results from calibration testing

Calibration Stage	Weight [g]	Calibration Force [mN]	Equivalent Thrust Force [mN]
1	4.07	46.11	20.49
2	9.51	93.31	41.47
3	14.40	141.27	62.79
4	19.27	188.97	83.98

From these numerical results, a calibration curve for a theoretical thruster positioned at the same 30.48 cm distance was created as shown in Fig. 10. The R^2 value from the linear fit was 0.994. Although these results were from an average on all damping cases, it isn't expected that the variance would change much for an individual damping case. Therefore, these results are satisfactory, but improvement is still possible with noise reduction algorithms and use of the inclinometer.

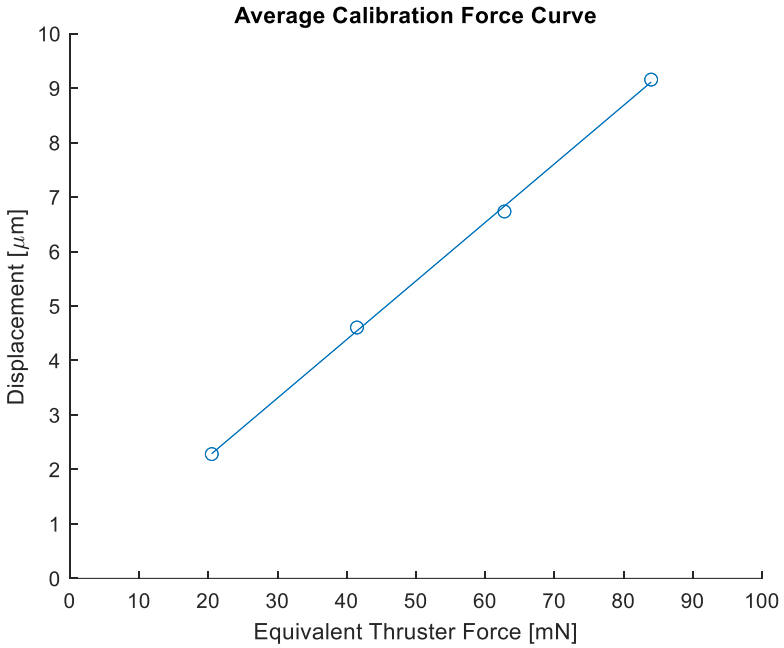

Fig. 10 Averaged calibration curve for an ideal thruster mounted 30.48 cm from rotational axis.

VI. Conclusion

A torsional thrust stand capable of measuring thrust from between 1 mN and 100 mN with the resolution of 0.1 mN was designed and developed for ALPE at WMU. The thrust stand was designed so that it can be modular and versatile for future testing on a variety of EP devices with varying thrust ranges. Future development of this thrust stand will include long-duration vacuum experiments to achieve zero drift testing. The first low thrust device that is planned to utilize this stand is a cold gas thruster operating at thrust levels between 50 mN and 100 mN. Potential improvements include the development of an active electromagnetic damping system, switching from manual micrometers to remotely controlled active leveling motors, and overall improvements on modularity. Long-term plans focus on increasing the optimal test range to accommodate low-thrust EP devices including miniature ion thrusters, Hall effect thrusters, and electron cyclotron resonance thrusters.

Acknowledgments

This work was supported by NSF through the Collaborative Research: CubeSat Ideas Lab: Space Weather Atmospheric Reconfigurable Multiscale Experiment (SWARM-EX) CubeSats, grant number 1936518.

References

[1] Tsukizaki, R., Koizumi, H., Nishiyama, K., and Kuninaka, H. "Plasma Diagnostics inside the ECR Ion Thruster μ10 by Laser Absorption Spectroscopy with Optical Fiber Probes," 48th Joint Propulsion Conference & Exhibit .2012. https://doi.org/10.2514/6.2012-4183

[2] Correyero, S., Jarrige, J., Packan, D., and Ahedo, E. "Plasma Beam Characterization along the Magnetic Nozzle of an ECR Thruster," Plasma Sources Science and Technology, Vol. 28, No. 9, 2019, p. 095004. https://doi.org/10.1088/1361-6595/ab38e1.

[3] Hu, J., and Rovey, J. L. "Faraday Cup with Nanosecond Response and Adjustable Impedance for Fast Electron Beam Characterization," Review of Scientific Instruments, Vol. 82, No. 7, 2011, p. 073504. https://doi.org/10.1063/1.3610649.

[4] Escobar, A. C. "A Langmuir Probe Instrument for Research in the Terrestial Ionosphere". Master of Science. The Pennsylvania State University, 2009.

[5] Polk, J. E., Pancotti, A., Haag, T., King, S., Walker, M., Blakely, J., and Ziemer, J. "Recommended Practice for Thrust Measurement in Electric Propulsion Testing," Journal of Propulsion and Power, Vol. 33, No. 3, 2017, pp. 539–555. https://doi.org/10.2514/1.B35564.

[6] Polk, J. E., Haag, T., King, S., Walker, M., Blakely, J., and Ziemer, J. "Recommended Practices in Thrust Measurements," Presented at the International Electric Propulsion Congerence, Washington DC, 2013.

[7] Haag, T. W. "Thrust Stand for Pulsed Plasma Thrusters," Review of Scientific Instruments, Vol. 68, No. 5, 1997, pp. 2060–2067. https://doi.org/10.1063/1.1148097.

[8] Wang, J. Z., Bian, X., Li, Q., and Wu, J. H. "A Magnetic Damper for Low Temperature," AIP Advances, Vol. 10, No. 10, 2020, p. 105107. https://doi.org/10.1063/5.0018572.